IFCEE 2021

GSP 324

Earth Retention, Ground Improvement, and Seepage Control

Selected Papers from the
International Foundation Congress and Equipment Expo 2021
Dallas, Texas ■ May 10–14, 2021

Edited by

Chadi El Mohtar, Ph.D.;
Stacey Kulesza, Ph.D.; Tugce Baser, Ph.D.;
and Michael D. Venezia, P.E.

ASCE

G-I GEO-INSTITUTE

GEOTECHNICAL SPECIAL PUBLICATION NO. 324

IFCEE 2021

EARTH RETENTION, GROUND IMPROVEMENT, AND SEEPAGE CONTROL

SELECTED PAPERS FROM SESSIONS OF THE INTERNATIONAL FOUNDATIONS CONGRESS AND EQUIPMENT EXPO 2021

May 10–14, 2021
Dallas, Texas

SPONSORED BY
International Association of Foundation Drilling
Deep Foundations Institute
Pile Driving Contractors Association
The Geo-Institute of the
American Society of Civil Engineers

EDITED BY
Chadi El Mohtar, Ph.D.
Stacey Kulesza, Ph.D.
Tugce Baser, Ph.D.
Michael D. Venezia, P.E.

Published by the American Society of Civil Engineers

Performance of the Wet Soil Mixing-Supported West Dowling Bridge during the 30 November 2018 Anchorage Earthquake

Armin W. Stuedlein, Ph.D., P.E.[1]; Matthew D. Gibson, Ph.D., P.E.[2]; Kenji Yamasaki, P.E.[3]; David Hemstreet, G.E., P.E.[4]; and Lisheng Shao, Ph.D., G.E., P.E.[5]

[1]Professor, School of Civil and Construction Engineering, Oregon State Univ., Corvallis, OR. Email: Armin.Stuedlein@oregonstate.edu
[2]Principal, Clarity Engineering LLC, Vashon, WA. Email: Matt@clarityengineering.net
[3]Geotechnical Engineer, U.S. Army Corps of Engineers, Portland, OR. Email: Kenji.j.Yamasaki@usace.army.mil
[4]State Foundation Engineer, Alaska Dept. of Transportation and Public Facilities, Anchorage, AK. Email: Dave.Hemstreet@alaska.gov
[5]Chief Engineer, Keller North America, Inc., Santa Paula, CA. Email: LShao@keller-na.com

ABSTRACT

The performance of improved ground during earthquakes continues to receive high interest in the geotechnical earthquake engineering profession given the need to establish best design and construction practices associated with ground improvement technology. The M7.1 30 November 2018 Anchorage earthquake produced significant shaking intensity at the West Dowling Street Bridge as recorded at a nearby ground motion station. The paper describes the site and subsurface conditions at the bridge, the static and seismic design objectives, and the deep soil mixing ground improvement used to satisfy performance criteria. Then, an overview of the 30 November 2018 earthquake is described, followed by an exploration of the ground motion characteristics measured 0.6 km from the bridge. Observations on the bridge condition conducted following the earthquake by members of the Alaska Department of Transportation and GEER association are described within the context of the measured ground motions. The paper concludes with Newmark-type seismic stability analyses conducted using the nearby ground motions to compare anticipated displacements with those observed following the earthquake. This case history provides a successful example of a shallow foundation-supported bridge abutment overlying deep soil mixing-improved ground and subjected to intense, directional ground motions.

INTRODUCTION

Deep soil mixing (DSM) ground improvement has been increasingly specified for strengthening of liquefiable and cyclic softening-susceptible ground, due in part to the continued improvement in the understanding of the intensity of expected seismic loading. The method, which generally consists of mechanical mixing of the native subgrade soils with cementitious slurry to produce a soil-cement or soil-crete columns or panels, is particularly attractive for highly-interlayered soil profiles that may exhibit both “sand-like” or “clay-like” behavior during cyclic loading, such as interbedded deposits of sands, non-plastic silts, and low-plasticity and plastic silts and clays which are difficult or impossible to densify using other ground improvement techniques. DSM ground improvement was used to improve the subgrade below the spread footing-supported substructure of the West Dowling Street Bridge in Anchorage,

Alaska, as described by Yamasaki et al. (2015). The goal of the ground improvement program was to improve construction stability and mitigate liquefaction and cyclic softening-induced deformations of shallow, non-plastic silts derived from glacial drift deposits, and facilitate use of spread footings as part of the bridge substructure.

A moment magnitude, M_w, 7.1 earthquake struck the City of Anchorage at 8:29 AM on 30 November 2018, just three years following construction of the West Dowling Street Bridge. This paper describes some of the observations of performance at this bridge during the earthquake and compares the performance to stability and simplified deformation analyses conducted following the earthquake. First, the site and subsurface conditions are presented. Then, the basis for seismic design is summarized. The observations made during post-earthquake reconnaissance conducted at the bridge by members of the Alaska Department of Transportation (AKDOT) and the Geotechnical Extreme Events Reconnaissance (GEER) Association are summarized. Limit equilibrium pseudo-static stability and Newmark-type (sliding block) deformation analyses using the motions recorded at a nearby seismic station are presented. This paper intends to provide a useful reference for those practitioners considering the use of DSM ground improvement.

SITE AND SUBSURFACE CONDITIONS

The West Dowling Street Bridge is situated approximately 8 km south of the Anchorage city center and serves to connect the C Street intersection to the east with Raspberry Road to the southwest. The super-elevated bridge provides an overpass for Arctic Boulevard and tracks owned by the Alaska Railroad, and consists of a single span, 30 m wide and 61 m long steel box girder-type superstructure. Reinforced concrete (R/C) shear keys provide transverse restraint to the R/C diaphragms and elastomeric bearing pad-supported box girders. Each substructure consists of reinforced concrete, cantilever retaining wall ranging from 11.9 to 13.5 m in height measured from the top of the spread footing serving as its foundation. The 1.2 m thick spread footings are 7.3 m wide by about 38 m long, and are founded on combination of mass-stabilized DSM and DSM shear panels, as described in detail below. Mechanically-stabilized earth (MSE) walls transitioning to R/C wing walls retain the approach fills.

Subsurface investigations in proximity to the bridge abutments and approach fills consisted of five boreholes and two penetrometer tests (Fig. 1). The Alaska Penetrometer Test (APT) consists of driving a 64 mm diameter steel rod with blunt tip with a 1.5 kN hammer (AKDOT 2007); the penetration resistance consists of the number of blows to drive the rod 0.3 m. Near-surface glacially-derived Holocene deposits (e.g., < 10 m depth; Yamasaki et al. 2015) varied in thickness and composition below the footprints of the bridge abutments. The pre-construction subsurface profile may be generalized as consisting of 0.9 m of fill (sand to gravel with silt and sand), underlain by peat (organic content about 74%) and sandy and silty clay to a depth of 3.35 m. This shallow peat and sandy and silty clay layer can be seasonally frozen, as was encountered during explorations at the end of March. Loose to medium dense, non-plastic to low-plasticity silt and silt with sand with uncorrected blow counts ranging from 5 to 15 extend to a depth of 8.5 m where the soils transition to a dense layer of sandy silt to silty sand that extend to a depth of 22 m. This deposit was underlain by a 10 m thick layer of medium stiff to very stiff, plastic, lightly-overconsolidated Bootlegger Cove clay (clayey silt to silty clay) followed by dense to very dense silty and sandy gravels interpreted as Pleistocene-age glacial till (Yamasaki et al. 2015). Groundwater was typically encountered at a depth of 3 to 7 m below the original ground surface.

The near-surface peat-rich soils were excavated within, and adjacent to, the footprint of the abutment footings. The deeper loose to medium dense non-plastic and low-plasticity silt layer was deemed too deep to cost-effectively excavate. The average fines content of the silt layer was 93%, with the water contents ranging from 20 to 30% and generally exceeding the liquid limit. Laboratory tests performed on samples collected in this silt layer from borings advanced to support design of the ground improvement indicated plasticity indices (PIs) of 0 to 4, indicating the potential for exhibiting "sand-like" behavior during cyclic loading. The average and standard deviation of the clean-sand, overburden stress-corrected standard penetration test (SPT) blow count, $N_{1,60cs}$, were calculated following Boulanger and Idriss (2014) to be 23 and 7.5 bpf, respectively. This range of relative density results in the potential for liquefaction under the design seismic loading, as described below. SPT-based correlations suggest that the shear wave velocity of the loose to medium dense, non-plastic silt deposit was approximately 190 m/s.

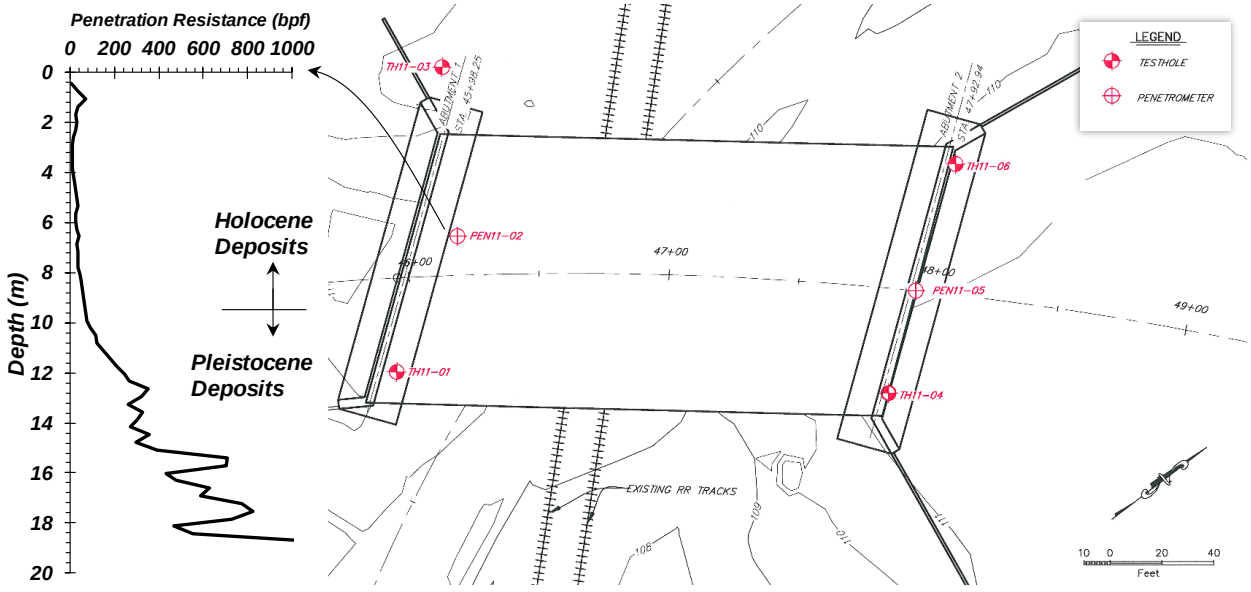

Fig. 1 Site and exploration plan for the West Dowling St. overpass (modified from AKDOT 2013a).

SEISMIC DESIGN AND DEEP SOIL MIXING PROGRAM

The seismic hazard governing the design of the ground improvement program included two scenario earthquakes drawn from the AKDOT Structural Foundation Engineering Final Report (AKDOT 2013b) and the probabilistic seismic hazard analysis derived from the USGS interactive deaggregation tool (Wesson et al. 1999). The first and contributing to approximately 9% of the overall seismic hazard, was a M9.2 megathrust earthquake, occurring at distance of approximately 55 km and producing a mean peak ground acceleration (PGA) of 0.27*g*. The second scenario was from shallow, random sources contributing about 47% of the seismic hazard with a magnitude range of M5 to M7.3, distance of about 9 km, and a mean plus one standard deviation PGA of 0.48*g*. The design PGAs were based on the Site Class D designation and Table 3.10.3.2-1 of AASHTO (2008). The 30 November 2018 earthquake, described below, consisted of a M7.1 intraslab event.

Liquefaction triggering analyses considering the substantial fines content conducted using the simplified method (Youd et al. 2001) indicated that the factor of safety against triggering of liquefaction for much of the loose to medium dense silt deposit would be less than 1.0 for both earthquake scenarios (Yamasaki et al. 2015). Further consideration of the driving static shear stress imposed by approach fill led the design team to conclude that the potential for strength loss and large deformations was significant and required remedial measures. Pseudo-static and post-liquefaction stability analyses of the unimproved subgrade conducted by the design team, including strength reductions to account for raised excess pore pressures and large strain potential, produced factors of safety of 1.0 and 0.80, respectively.

The use of deep foundations to support the bridge substructure was considered costly given the approximately 34 m depth to the dense to very dense till that could serve as the bearing layer for deep foundations, static downdrag-induced dragloads due to consolidation of the Bootlegger Cove formation, long-term differential settlement between the approach and the abutment, and post-liquefaction dragloads. Following the evaluation of several ground improvement alternative methods as described by Yamasaki et al. (2015), deep soil mixing was selected to: (1) mitigate liquefaction of the silts, (2) improve post-shaking stability, (3) economically support the bridge abutments on spread footings, (4) reduce the differential settlement between the bridge foundations and the approach fills, and (5) limit impact to the nearby railroad tracks and other buried utilities including a gas and water line, storm sewer, and fiber optic cable. The wet deep soil mixing program was designed to mix cement slurry with the loose to medium dense silt layer to form two treatment zones using 2.44 m diameter soil-crete columns, overlapping by 0.15 m, to a depth of 9 m. The inner treatment zone below the spread footing and the outer treatment zone extended out beyond the footing was designed with an area replacement ratio, a_r, equal to 90% and 50%, respectively.

Figure 2 presents construction drawings for the DSM ground improvement. The inner DSM treatment zone with a_r = 90% extends 2.3 m beyond the edges of the spread footings. The outer DSM treatment zone with a_r = 50% extends horizontally to a distance of 10.7 m in front (track-side), and 9 m beyond the sides and rear, of the footing edges. Following installation of the DSM, the soil above the treatment zones was excavated and replaced with compacted aggregate base course of approximately 1.8 m thickness that provides direct support of the spread footing. This configuration was designed to: (1) provide a stiffened subgrade below the zones of greatest stress intensity resulting from the abutment loading, and (2) improve global stability as described by Yamasaki et al. (2015). Based on the experience of the geotechnical specialty contractor, the a_r specified, and the strength of the native soils, a design composite shear strength of 190 kPa was used for both DSM treatment zones. Global stability factors of safety using these design strengths increased to 1.2 for a pseudo-static scenario considering a design horizontal seismic coefficient of 0.23 and 1.8 for a post-shaking scenario considering liquefaction outside of the improved zone (Yamasaki et al. 2015). The seismic coefficient was controlled by the shallow random earthquake scenario, a tolerable deformation of 25 to 50 mm, and was determined from the procedures outlined by Anderson et al. (2008).

A total of 511 2.44 m diameter DSM columns were constructed in 32 days. Seventy-five sets of wet samples were retrieved following mixing and tested to document the unconfined compressive strength (UCS) and its variation at 3, 7, 14, 28, and 56 days of age (ASTM D1633; ASTM 2017). A statistical analysis on the 56-day UCS is presented in Figure 3. The wet samples retrieved from the field-installed DSM columns exhibited an average UCS equal to twice the

design target of 1.03 MPa (150 psi), with just 4% of samples exhibiting a UCS less than the design strength.

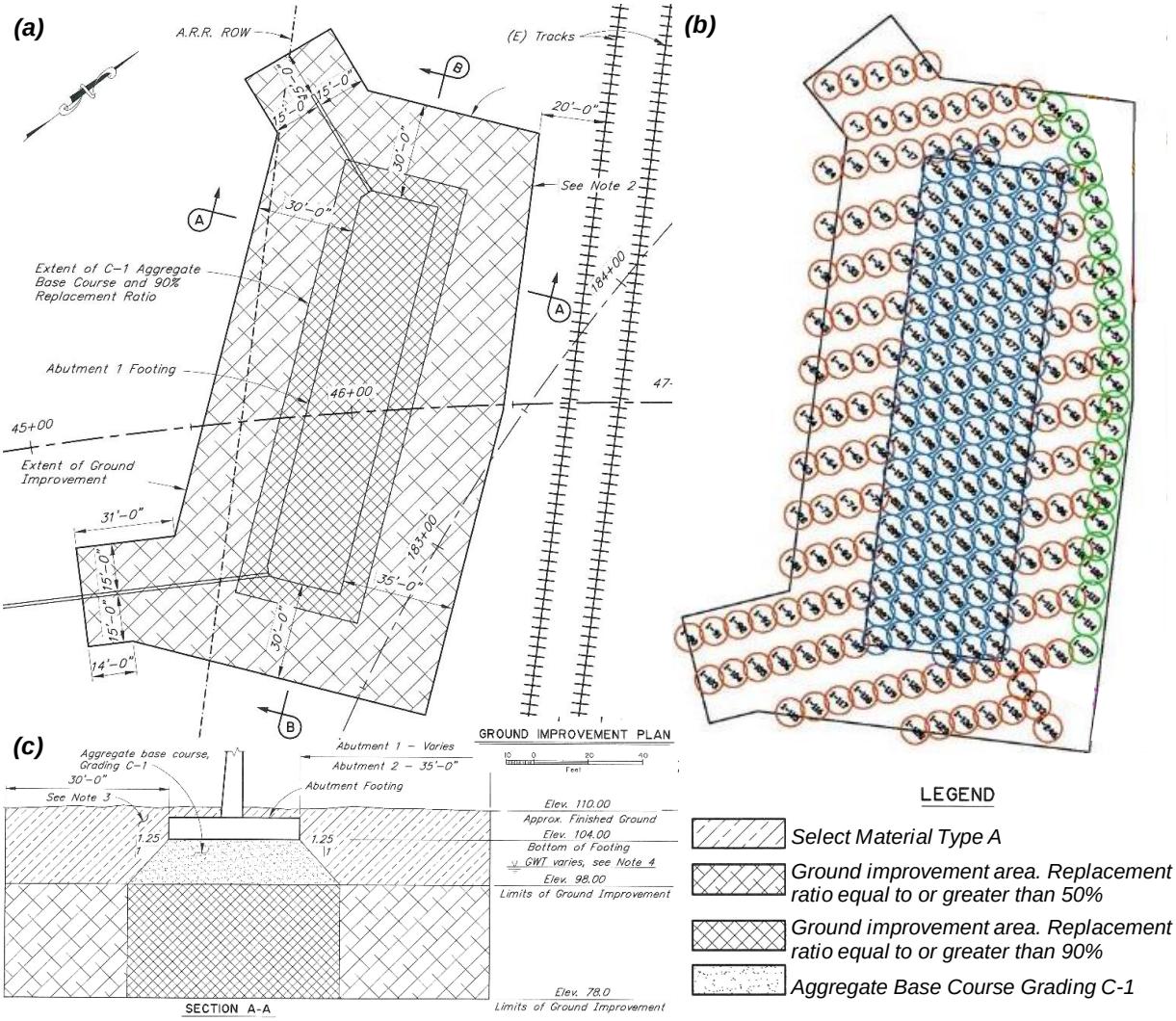

Fig. 2 Wet soil mixing ground improvement program below the left bridge abutment, indicating: (a) plan view of treatment extent and spread footing, (b) distribution of overlapping 2.44 m diameter DSM columns in the form of mass-stabilization (a_r = 90%) and shear panels (a_r = 50%), and (c) Section A-A, with compacted aggregate base course overlying DSM treatment (modified from AKDOT 2013a and Yamasaki et al. 2015).

30 NOVEMBER 2018 ANCHORAGE EARTHQUAKE

Overview of the Earthquake and Observations: A M7.1 earthquake shook the City of Anchorage at 08:29 AM on 30 November 2018 with epicentral distance approximately 11 km north of the downtown (Cabas et al. 2020). The normal faulting instraslab event occurred at a hypocentral depth of approximately 47 km within the Pacific plate, which is being subducted

below the North American plate along the Alaska-Aleutian subduction zone at the rate of about 5.1 cm/year (West et al. 2020), and ruptured upwards along a plane with length of 25 to 35 km (Franke et al. 2019). More than 9,000 aftershocks followed the main shock, with 40 larger than M4, five larger than M5, and the largest equal to M5.7 just minutes after the mainshock. Most of the ground motion stations within the city recorded PGAs ranging from 0.2 to 0.3*g*; however, the station nearest the West Dowling Street Bridge registered a PGA = 0.47*g*, similar to the design earthquake scenario controlling slope stability. Members of the Geotechnical Extreme Events Reconnaissance (GEER) Association summarized many observations made in the weeks immediately following the event, including (Franke et al. 2019; Cabas et al. 2020):

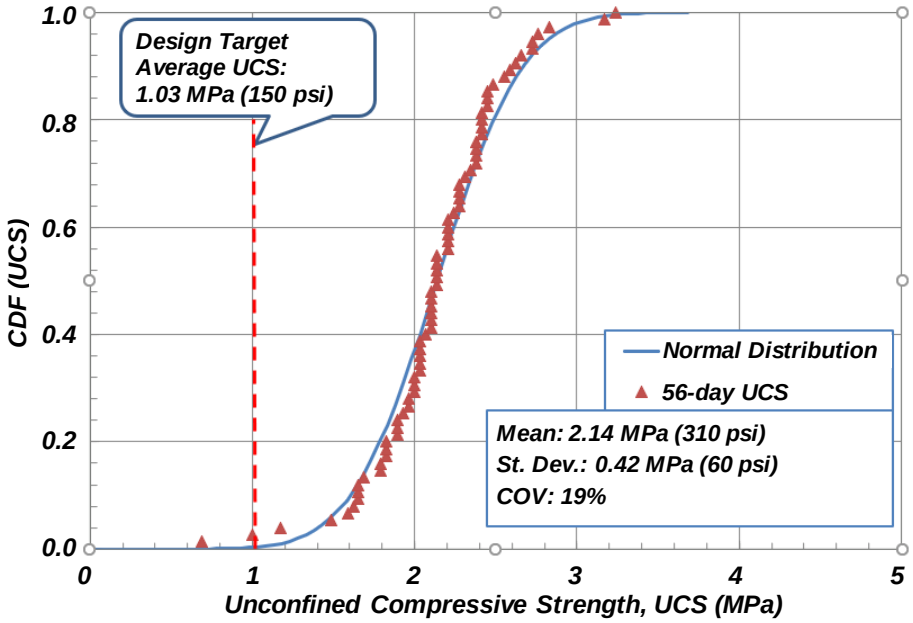

Fig. 3 Statistical distribution of the unconfined compressive strength of wet samples taken from the DSM at 56 days.

- The 2018 Anchorage earthquake was one of the strongest earthquakes to hit a major US city since the 1994 Northridge earthquake;
- Modified Mercalli Intensities (MMI) of VII were experienced throughout the city;
- Amplification of the ground motions varied considerably in the Anchorage basin;
- Ground motions did not generally exhibit strong directionality, except for Station NSMP 8027 – the instrument located nearest to the West Dowling Street Bridge;
- The duration of the earthquake, relatively short, contributed to relatively small amount of damage observed following the earthquake.

Ground failure consisted of liquefaction as evidenced through sand boils and settlements of structures and lateral spreads, and failure of anthropogenic fills and embankments, particularly those overlying peaty and organic soils and along coastal bluffs (Franke et al. 2019; Cabas et al. 2020).

Characteristics of the Measured Ground Motions at Station NSMP 8027: Station NSMP 8027, located in a warehouse immediately north of the Alaska Department of Fish and Game (Latitude 61.1609°, Longitude –149.8894°), is situated approximately 0.6 km south from the

West Dowling Street Bridge. This location corresponds to the western boundary of NEHRP Site Class C/D and D contours within the Anchorage Basin proposed by Martirosyan et al. (2002). Figure 4 presents the acceleration response spectra, acceleration time histories, and Arias Intensities, *AI*, of the two horizontal components of shaking recorded at the station. These motions have been baseline corrected and filtered with a Butterworth bandpass filter at 0.1 and 25 Hz. Unlike most of the recordings in Anchorage, this station recorded strong directionality effects, with the east-west (HNE) component exhibiting significantly stronger intensity (e.g., PGA = 0.47*g*, *AI* = 1.87 m/s) than the north-south (HNN) component (with PGA = 0.19*g*, *AI* = 0.66 m/s). As a result, the bridge was loaded out-of-plane with its alignment and approaches, experiencing significant transverse motion. Furthermore, inertial loading experienced by the bridge would likely have been amplified given the typical natural periods of stiff, single-span bridges and the pseudo-spectral acceleration response presented in Fig. 4. Evidence of such loading is described below.

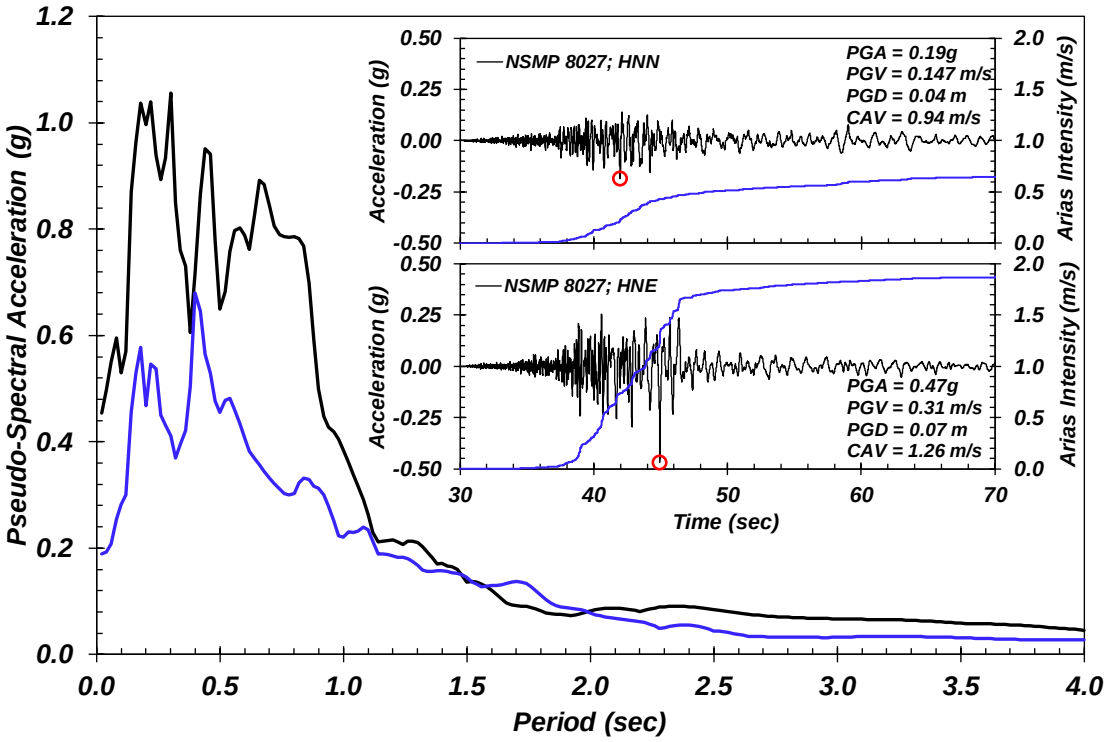

Fig. 4 Response spectra, baseline corrected acceleration time histories, and Arias Intensities for the north-south (HNN) and east-west (HNE) components of ground motion at Station NSMP 8027, located approximately 0.6 km from the West Dowling Street Bridge.

Observations by the GEER team following the earthquake noted maximum settlements of about 160 mm at a nearby structure within 150 m of the station, with reports of 300 mm of settlement occurring within the footprint of the structure. Such deformations are indicative of the strength of shaking and the liquefaction, cyclic softening, or seismic compression of the underlying soils. Liquefaction (or cyclic softening) has been observed to affect the frequency content of measured ground motions as the softening of soil due to the generation of excess pore

pressures results in the inability to transmit higher frequencies (Kramer et al. 2016). Stockwell spectrograms can be used to observe the evolution of frequency content within a recorded motion and potentially identify the effects of liquefaction on the ground motion characteristics as well as the time of liquefaction (Ozener et al. 2020). Figure 5 presents the Stockwell transform of the HNE component of the ground motion recorded at NSMP 8027. Initially high frequencies (e.g., greater than 10 Hz) in the time ranging from 30 to 35 s gradually reduce from the period of 35 to 44 s, indicating a softening of the soil under the recording station. Thereafter, the transmitted frequencies generally consist of a narrow band ranging from about 0.8 to 3.2 Hz (*n.b.*, surface wave may have initiated at approximately 51 s); such frequencies have been associated with liquefaction/cyclic softening of the underlying soil (Kramer et al. 2016; Ozener et al. 2020) and are consistent with the observations of large settlements near the recording station described above, indicating that the similarity in characteristics of 30 November 2018 earthquake with the design shallow, crustal earthquake scenario would have likely produced liquefaction/cyclic softening at the West Dowling Street Bridge in the absence of ground improvement.

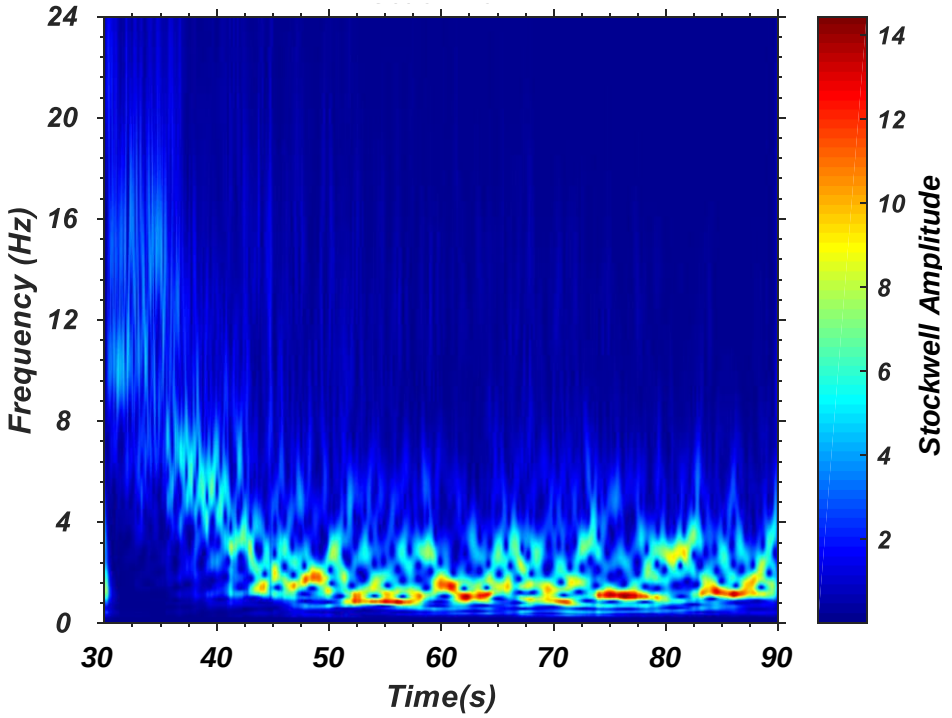

Fig. 5 Stockwell spectrogram of the HNE component of the ground motion at Station NSMP 8027, indicating a reduction in frequency content consistent with the softening of soil in the underlying soil.

OBSERVATIONS FOLLOWING THE ANCHORAGE EARTHQUAKE

Observations of the Superstructure: Bridge inspections performed by the AKDOT (Escamilla 2018) and reconnaissance by members of the GEER team (A.W. Stuedlein, C.Z. Beyzaei, and K. Lee) occurred on 4 December and 10 and 12 December, 2018, respectively. In

general, light damage was noted in the field relative to the intensity of shaking the bridge likely experienced. Evidence of possible pounding of the bridge deck and abutment at the northeast transition from the approach fill to the superstructure could be observed from diagonal shear cracking of the abutment at the location of an expansion joint (Fig. 6a, 6c), along with 25 mm of permanent transverse movements (Fig. 6a), or approximately 1/3 of the peak ground displacement, *PGD*, in the HNE component of the corrected motion (Fig. 4). Near the same location, cracks in the reinforced concrete wingwall and exterior face of the diaphragm were noted (Fig. 6b). Spalling and/or delamination of concrete at several shear keys at the abutments was noted suggesting transverse interaction of the abutment and superstructure (Fig. 6d). These observations were confirmed by permanent out-of-plane deformation of steel I-sections supporting guardrails at the top of the bridge.

Observations of the Substructures: The AKDOT inspections revealed that expansion bearings appeared fully-extended with little capacity to accommodate additional movement, suggesting that the abutments may have displaced towards one another. The tilt of the abutments was measured by members of the GEER team, and indicated that the southwest abutment rotated away from the approach fill by a maximum of 1.1 degrees at the eastern end and transitioning to 0.4 degrees at the western end. The northeast abutment rotated 0.4 degrees towards the bridge deck at the western end and zero along the eastern end. These observations appear to confirm those regarding movement of the abutments by members of the AKDOT. Concrete MSE wall fascia panels retaining the approaches exhibited minor spalling. Evidence for closure and extension between gaps separating adjacent panels was noted, with movements of up to 75 mm and tilt of approximately 4 degrees (Figs. 6e, 6f, and 6g). Elastomeric bearing pads placed to reduce stress concentrations between adjacent and overlying panels alternately exhibited compression or unloading as a function of in-plane tilt. An unretained slope at the southern end of the eastern approach exhibited approximately 100 mm of lateral movement and a 300 mm vertical scarp, with rotation of planted saplings providing further evidence for the minor slope failure.

Discussion: No significant evidence for differential settlement or ground failure (e.g., manifestation of liquefaction) was noted along, adjacent to, or within the retained approach fill and abutments. While the evidence for pounding suggests that rocking of the DSM-supported spread footings may have been possible, all of the observations point towards a satisfactory performance of the bridge given that the PGA recorded approximately 0.6 km away was approximately equal to the design PGA controlling slope stability.

On the other hand, the significant duration of approximately 25 seconds for this earthquake was shorter than that expected for the governing design subduction zone earthquake. The lower significant duration also implies a fewer number of strong cycles of loading that may have prevented significant loss of strength of the untreated surficial and non-plastic to low plasticity soils and is evident with the lack of significant observable permanent deformation of the approach fills. This suggests that PGA may not best represent the overall damage potential of an earthquake, as pointed out by others (e.g., Jibson et al 2000, Bullock et al. 2018). However, as noted earlier, effects consistent with liquefaction observed nearby (e.g., settlements of 300 mm near station NSMP 8027 and significant reductions in the frequency content of recorded motions shown in Fig. 4) compared to those effects predicted during design for the similar design ground motion scenario suggests that efforts to mitigate for liquefaction at the West Dowling Street Bridge were well-substantiated.

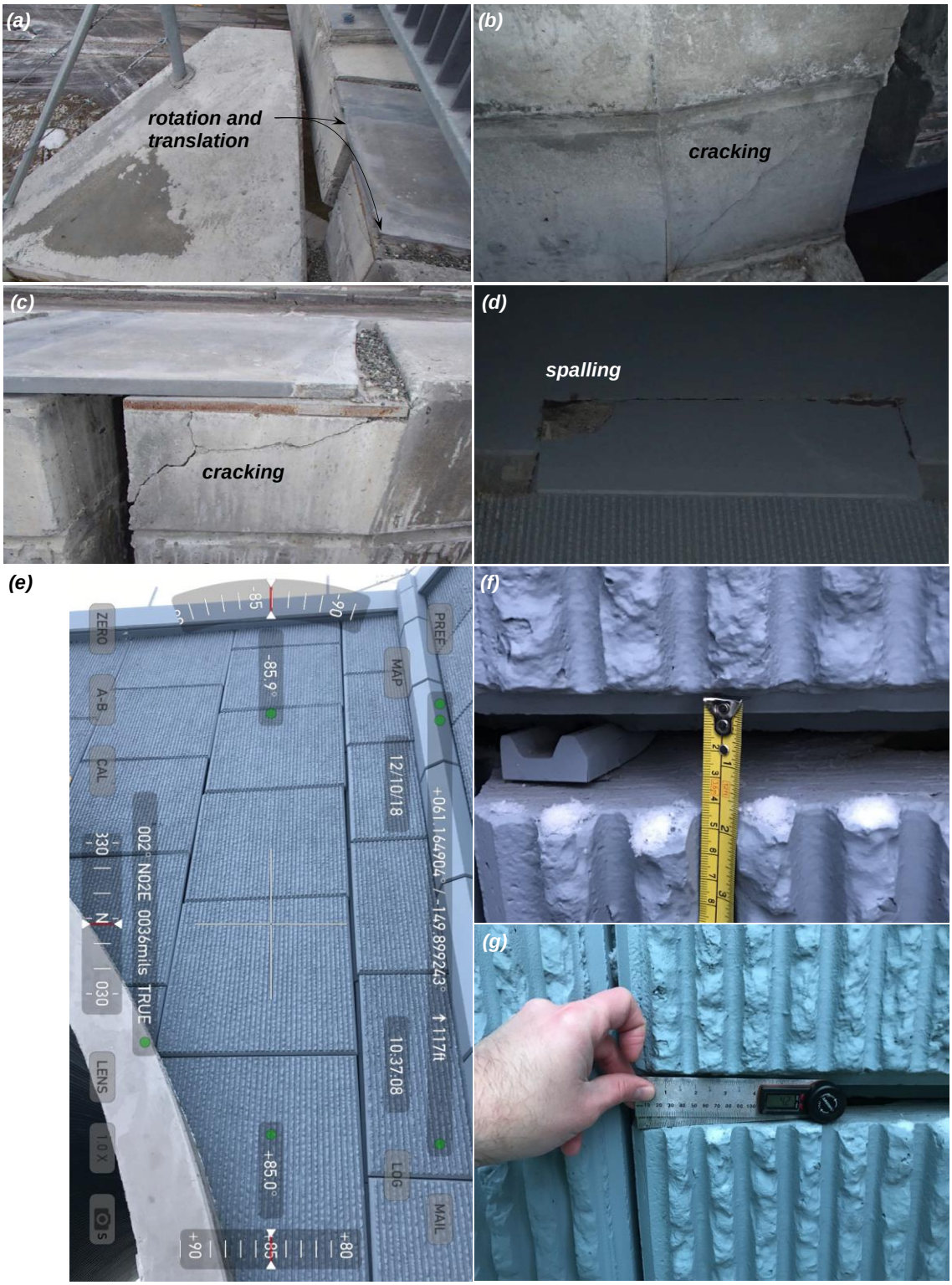

Fig. 6 Photographs taken by AKDOT inspectors and GEER team members: (a) translation and rotation of northeast abutment relative to deck, (b) exterior face of diaphragm, (c) evidence of pounding at northeast abutment, (d) spalling along shear key, (e) rotation of approach fill MSE wall fascia panels near culvert, (f, g) differential movement and rotation of MSE wall panels, approach fill.

PSEUDO-STATIC STABILITY AND DISPLACEMENT ANALYSES OF 2018 EARTHQUAKE

Seismic performance of the approach fill and abutment under the 2018 earthquake was evaluated using pseudo-static slope stability evaluations, sliding block time history analyses, and empirical sliding block models to assess the results from typical procedures used in geotechnical engineering practice. In the following, it is assumed that the ground motion recorded at NSMP 8027 represents the unobserved motions at the West Dowling Street Bridge site; furthermore, these analyses do not consider the potential diaphragm or pinning action provided by the bridge deck between the two abutments.

Pseudo-Static Slope Stability: The original ground improvement design considered a horizontal seismic coefficient of 0.23*g* with the assumption that deformation of 50 mm or less was acceptable. Figure 7 presents the slope stability model evaluated along with the strength parameters used in the analyses. The slope stability analyses along the longitudinal direction of the abutment produced a critical horizontal yield acceleration of 0.31*g*. Although both the design and as-built DSM strengths were considered in the pseudo-static stability analyses, the large strengths of the DSM-improved zone relative to the backfill soils forced the critical yield surface into the fill above the DSM and behind the abutment as designed. Note that if concrete-soil interface friction along the base of the footing is considered (and set equal to 28 degrees), then the critical yield acceleration reduces to 0.28*g*. The yield acceleration for a slip surface through the DSM at strengths considered during design is about 0.4*g*.

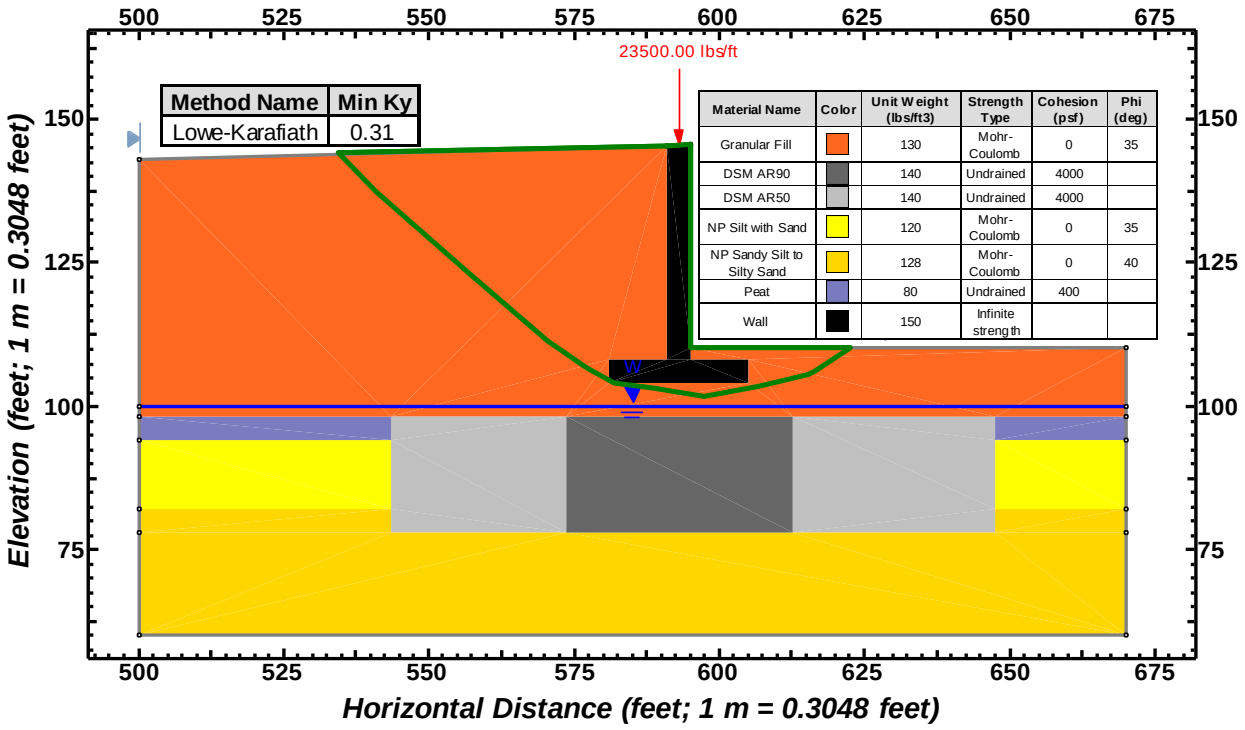

Fig. 7 Pseudo-static slope stability evaluation to determine critical horizontal yield acceleration. The DSM shear strength is sufficient to produce a critical slip surface within the fill. Note that block slip surfaces were also evaluated and returned similar critical horizontal yield accelerations. Note: 1 m = 3.28 ft; 1 kPa = 20.9 psf ; = 1 kPa; 1 KN/m^3 = 6.24 lbs/ft^3.

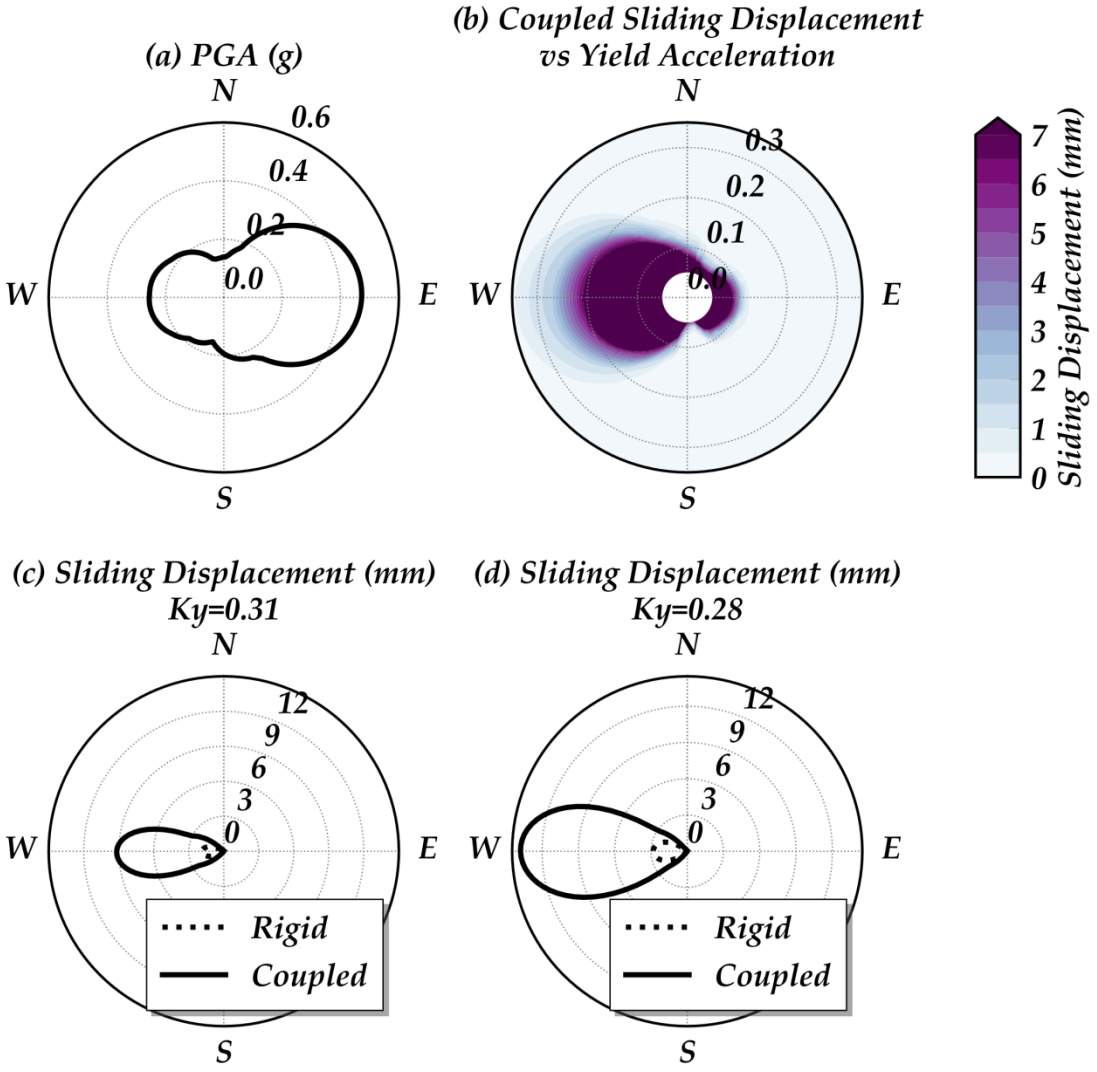

Fig. 8 Azimuthal variation of PGA and dynamic sliding block displacements: (a) peak ground acceleration, (b) coupled sliding displacements as a function of horizontal yield acceleration, (c) rigid and coupled displacements for a horizontal yield acceleration of 0.31*g*, and (d) rigid and coupled sliding displacement for a horizontal yield acceleration of 0.28*g*.

Dynamic Sliding Block Deformations: To assess sliding displacement potential of the abutment, rigid and coupled sliding block analyses were performed using each ground motion pair as input at the base of the slide mass. The program SLAMMER (Jibson et al. 2013) was used to calculate the displacements. For the coupled analyses, the following input was used: (1) abutment height equal to 13 m, (2) a strain reduced slide mass shear wave velocity, V_s, equal to 225 m/s, (3) V_s below slide mass equal to 400 m/s, (4) damping ratio equal to 2%, (5) linear-elastic behavior, and (6) horizontal yield acceleration of 0.31*g* and 0.28*g*. Because the bridge and ground motion orientations are not identical, the PGA and sliding displacements were calculated for various orientations of the ground motion. Figure 8a presents the variation in expected PGA

with azimuthal bearing illustrating the degree of directionality in the motion intensity that the bridge was likely to have been subjected. Figure 8b presents the azimuthal variation of the horizontal yield accelerations and the variation of the corresponding coupled sliding displacements. For ease of interpretation, Figure 8c and 8d present the azimuthal variation of rigid and coupled sliding displacements for the two horizontal yield accelerations considered (i.e., 0.31 and 0.28g). These results illustrate the influence of ground motion directionality on sliding displacements with the maximum ground acceleration oriented to the east and thus the maximum sliding potential oriented towards the west. These analyses resulted in permanent displacements of 2 mm for the rigid analysis and 9 mm for the coupled analysis for the higher yield acceleration and the HNE component. The lower yield acceleration yields rigid and coupled displacements of 3 and 14 mm, respectively.

Empirical Sliding Block Deformations: Sliding deformations were also estimated using empirical methods by Bray and Travasarou (2007) and Rathje and Antonakos (2011). For the Bray and Travasarou method, a fundamental abutment period, T_s, of 0.2 seconds and spectral acceleration ($S_a(1.5\ T_s)$) of 1.0g was assumed, and produced a median estimated lateral displacement of 80 mm and a probability of exceeding 70 mm of deformation was 57 percent. For the Rathje and Antonakos method, and with the additional assumption of a mean shaking period, T_m, of 0.7 seconds, the displacement was estimated to be about 15 mm.

Discussion: The light damage to transverse shear keys and permanent relative displacements between the bridge deck and abutment noted above (approximately 25 mm) point to the relative accuracy of the coupled sliding displacement and Rathje and Antonakos (2011) models. However, the recorded ground motions appear to have been affected by softening or liquefaction of the soils at the ground motion recording station, as noted above. Compared to the DSM-improved ground installed to mitigate against softening behavior, the use of the ground motions from the recording station likely results in an underestimate of the overall intensity of the ground motion experienced at West Dowling Street Bridge. For this reason, the sliding displacements estimates presented here likely represent a lower bound estimate. In addition, it is possible that the restraint created by the bridge deck may have mitigated some of this translational potential into the rotational deformation that was observed following the earthquake.

These analyses illustrate two additional points: (1) the east-west, directional nature of the ground motion likely impacted the bridge obliquely to the longitudinal direction of the bridge, and (2) the importance in considering site response (e.g., amplification) that may have increased the sliding deformation potential of the abutment. Lastly, the comparison of sliding displacements computed from the time history analyses to those estimated using the selected empirical methods point to the need for accurately parameterizing, and therefore predicting, the spectral shape of the ground motion in order to obtain accurate sliding predictions.

CONCLUDING REMARKS

The M7.1 30 November 2018 Anchorage earthquake produced intense, directional shaking of the West Dowling Street Bridge in Anchorage, Alaska and an opportunity to examine the full-scale response of a single-span bridge overlying improved ground. The near-surface soils consisted of non-plastic to low-plasticity silts that were deemed susceptible to liquefaction and potentially liquefiable under various design-level earthquakes. Deep soil mixing (DSM) was used to mitigate static and seismically-induced deformations and support the bridge on economical shallow foundations. An assessment of the strength of DSM samples taken from the field indicated that the 56-day unconfined compressive strength was twice the design strength.

Ground motions recorded approximately 0.6 km from the bridge site indicate strong directionality, with the largest component of shaking in the east-west direction. Observations of the seismic performance of the bridge sub- and super-structures indicate possible evidence for pounding of the abutment and bridge deck, with spalling of concrete at the transverse shear keys that were consistent with the recorded directionality of the ground motions. No evidence for differential settlement or ground failure was noted along or within the retained approach fill and bridge abutments. All of the post-event observations point towards a satisfactory performance of the bridge given that the recorded PGA was approximately equal to the design PGA controlling slope stability. The assessment of rigid Newmark-type, coupled, and empirical sliding displacement methods that incorporated the measured ground motions and critical yield surface indicated a relatively large range in expected displacements (i.e., 2 to 80 mm) depending on the assumptions corresponding to each method. The relatively light damage to elements of the superstructure and lack of evidence of ground failure point to the relative accuracy of the coupled sliding displacement and Rathje and Antonakos (2011) methodologies. Given that DSM ground improvement was present below the bridge substructure and not present at the recording station, the intensity of shaking may have been larger at the bridge since the recordings may have been affected by significant softening of the subsurface below the seismic station. It is emphasized that ground improvement is used to stiffen the improved soil profile to reduce seismic deformations; a consequence of increased stiffness is the change in the fundamental frequency of the soil profile and the potential for increased inertial loading over a certain range in motion frequencies (and a reduction in inertial loading over a separate range of frequencies) relative to the pre-improvement condition which are best judged on a case-by-case basis. This case history demonstrates that the DSM ground improvement and shallow foundations served to prevent significant deformations and temporary closure of the West Dowling Street bridge following the 30 November 2018 Anchorage earthquake.

ACKNOWLEDGEMENTS

Funding to support the reconnaissance of Anchorage and the neighboring communities following the 30 November 2018 earthquake was provided to the lead author by the Geotechnical Extreme Events Reconnaissance (GEER) Association, through the National Science Foundation under Grant No. CMMI-1266418, and is gratefully acknowledged. Any opinions, findings, and conclusions or recommendations expressed in this material are those of the authors and do not necessarily reflect the views of the NSF. The authors would like to acknowledge the GEER team, including Kevin Franke, Rich Koehler, Christine Beyzaei, Ashly Cabas, Sam Christie, Steve Dickenson, Ian Pierce, and Joey Yang. Kannon Lee assisted the lead author during the first visit to the West Dowling Street Bridge. The authors are grateful for the helpful discussions with and assistance provided by John Thornley.

REFERENCES

AASHTO. (2008). “AASHTO LRFD Bridge Design Specifications.” 2008 Interim Revisions, American Association of State Highway and Transportation Officials.

Alaska Department of Transportation (AKDOT). (2007). “Alaska Geotechnical Procedures Manual.” Alaska Department of Transportation and Public Facilities, Juneau, AK. 187 pp.

Alaska Department of Transportation (AKDOT). (2013a). "West Dowling Road Overcrossing." Construction Drawings, Bridge No. 2273, Alaska Department of Transportation and Public Facilities, Juneau, AK. 33 pp.

Alaska Department of Transportation (AKDOT). (2013b). "Final Structural Foundation Engineering Report, Dowling Road Overhead, Bridge No. 2273." Alaska Department of Transportation and Public Facilities, Anchorage, AK. 48 pp.

Anderson, D. G., Martin, G. R., Lam, I., and Wang, J. N. (2008). Seismic Analysis and Design of Retaining Walls, Buried Structures, Slopes, and Embankments. NCHRP Report 611, Transportation Research Board, Washington, D.C.

ASTM. (2017). *Standard Test Methods for Compressive Strength of Molded Soil-Cement Cylinders*. ASTM D1633-17, ASTM International, West Conshohocken, PA.

Boulanger, R. W., and Idriss, I. M. (2014). "CPT and SPT based liquefaction triggering procedures." Report No. UCD/CGM-14, University of California, Davis.

Bray, J. D., and Travasarou, T. (2007). "Simplified Procedure for Estimating Earthquake-Induced Deviatoric Slope Displacements." *Journal of Geotechnical and Geoenvironmental Engineering*, 133(4), 381–392.

Bullock, Z., Dashti, S., Liel, A., Porter, K., and Karimi, Z. (2018). "Efficiency, Sufficiency, and Predictability of Intensity Measures for Predicting Liquefaction Consequences." *Proc., 11th Nat. Conf. on Earthquake Engineering*, Earthquake Engineering Research Institute, Los Angeles, CA. 11pp.

Cabas, A., Beyzeai, C., Franke, K., Koehler, R., Pierce, I., Stuedlein, A. W., Yang, Z., and Christie, S. (2020). "Turning Disaster into Knowledge: Geotechnical Aspects of the 2018 Mw 7.1 Anchorage Alaska Earthquake." *2020 Geo-Congress*.

Franke, K. W., Koehler, R. D., Beyzaei, C. Z., Cabas, A., Christie, S., Dickenson, S., Pierce, I., Stuedlein, A., and Yang, Z. (2019). "Geotechnical Engineering Reconnaissance of the 30 November 2018 Mw 7.1 Anchorage, Alaska Earthquake," Geotechnical Extreme Events Reconnaissance Association, GEER Report No. 059, Version 2.

Jibson, R. W., Harp, E. L., and Michael, J. A. (2000). "A method for producing digital probabilistic seismic landslide hazard maps." *Engineering Geology*, 58(3–4), 271–289.

Jibson, R. W., Rathje, E. M., Jibson, M. W., and Lee, Y. W. (2013). "SLAMMER: Seismic Landslide Movement Modeled using Earthquake Records," Unitied States Geologic Survey Numbered Series, 12-B1, Version 1.1 revised November 2014.

Kramer, S. L., Sideras, S. S., and Greenfield, M. W. (2016). The timing of liquefaction and its utility in liquefaction hazard evaluation. *Soil Dynamics and Earthquake Engineering*, 91, 133-146.

Martirosyan, A., Dutta, U., Biswas, N., Papageorgiou, A., and Combellick, R. (2002). Determination of site response in Anchorage, Alaska, on the basis of spectral ratio methods, *Earthq. Spectra*, 18, 85–104.

Moschetti, M. P., Thompson, E. M., Rekoske, J., Hearne, M. G., Powers, P. M., McNamara, D. E., and Tape, C. (2020). Ground-Motion Amplification in Cook Inlet Region, Alaska, from Intermediate-Depth Earthquakes, Including the 2018 M w 7.1 Anchorage Earthquake. *Seismological Research Letters*, 91(1), 142-152.

Özener, P. T., Greenfield, M. W., Sideras, S. S., and Kramer, S. L. (2020). Identification of time of liquefaction triggering. *Soil Dynamics and Earthquake Engineering*, 128, 105895.

Rathje, E. M., and Antonakos, G. (2011). "A unified model for predicting earthquake-induced sliding displacements of rigid and flexible slopes." *Engineering Geology*, 122(1), 51–60.

Wesson, R. L., Frankel, A. D., Mueller, C. S., and Harmsen, S. (1999). Probabilistic Seismic Hazard Maps of Alaska, Open-File Report 99-36, U.S. Geological Survey.

West, M. E., Bender, A., Gardine, M., Gardine, L., Gately, K., Haeussler, P., and Tape, C. (2020). The 30 November 2018 M w 7.1 Anchorage earthquake. *Seismological Research Letters*, 91(1), 66-84.

Yamasaki, K., Hemstreet, D., Gerondale, A., and Shao, L. (2015). Wet soil mixing for supporting bridge abutments on spread footings. *Deep Mixing*, 2015, 395-404.